


 Cite this: *Chem. Commun.*, 2024, 60, 7578

 Received 10th May 2024,
 Accepted 19th June 2024

DOI: 10.1039/d4cc02282c

rsc.li/chemcomm

2D metal–organic frameworks bearing butterfly-shaped metal-bis(dithiolene) linkers from dithiol-functionalized benzenedicarboxylic acid†

 Hao Zhong,^a Zhixin Jiang,^a Jieying Hu,^a Lai-Hon Chung *^{ab} and Jun He *^{ab}

An assembly between 1,4-dicarboxylbenzene-2,3-dithiol (H₂dcbdt) and different transition metal ions successfully produced 2D metal–organic frameworks (M-dcbdt, M = Ni, Co or Fe) composed of unprecedented butterfly-shaped metal-bis(dithiolene) (MS₄) linkers in one-pot fashion. Such strategy provides easier access to the [MS₄]-rich network and lowers the prerequisite to explore their applications.

Metal-bis(dithiolene) is a class of square-planar complexes with the metal centre coordinated to four sulphur atoms of two bidentate ligands. Studies on them date back to the 1960s, over a half-century ago.¹ The noninnocence of metal-bis(dithiolene) promotes their unique properties in electrical conduction² and catalysis.³ Besides artificial structures, metal-bis(dithiolene) is ubiquitous in nature; for example, Mo-bis(dithiolene) units are active sites in dimethyl sulphoxide reductase (DMSOR).⁴ These attractions make metal-bis(dithiolene) a star in the scientific field, and fundamental as well as application studies of this giant continue unabated. However, the extensive studies of metal-bis(dithiolene) are focused on molecular analogues, which show limited regulation of electronic structures by editing functionalities (*e.g.*, separate orbitals), suffer low recyclability (being homogeneous), and have weak operational stability (vulnerable to surrounding chemical species).⁵

Inspired by nature, the incorporation of metal-bis(dithiolene) sites into frameworks (such as enzymes) sheds light on the retained activity and enhanced stability at the same time. Following this direction, the incorporation of metal-bis(dithiolene) in frameworks was first actualized by a series of metal-bis(dithiolene) bridged 2D conductive networks.⁶ Shifting from separate molecular metal-bis(dithiolene) to a continuous network transforms discrete orbitals to band structures, which determine the observed electrical conductivity. Beyond electrical conduction, Zou *et al.* invented

tetratopic Ni-bis(dithiolene) linkers to construct stable 2D or 3D frameworks and demonstrated their functions in different applications such as sensing,⁷ CO₂ reduction,⁸ batteries,⁹ and photothermal conversion¹⁰ with flying colours. These successful examples highlight the potential of the metal-bis(dithiolene) framework and support the search for a facile general approach to easily access such frameworks.

Herein, we report the use of a simple dithiol-functionalized benzene dicarboxylic acid as a building block to construct 2D frameworks bearing a butterfly-shaped metal-bis(dithiolene) node with different transition metal ions in one-pot manner. The assembly of such networks could also be achieved by starting from the butterfly-shaped metal-bis(dithiolene) metallolinker and shows generality (such methodology applicable to various transition metals, including Ni, Co or Fe). Resultant networks show satisfactory chemical stability and demonstrate photocatalytic activity in the hydrogen evolution reaction (HER). This work reports an unprecedented, simple way to obtain metal-bis(dithiolene)-rich metal–organic frameworks (MOFs) on demand (one-pot fashion for convenience or starting from butterfly-shaped metallolinker for functional design) and with generality (feasible for different transition metal ions).

A solvothermal reaction between 1,4-dicarboxylbenzene-2,3-dithiol (H₂dcbdt) and transition metal salts (Ni(OOCCH₃)₂·4H₂O, Co(OOCCH₃)₂·4H₂O or FeCl₃·6H₂O) with CH₃COOH as a modulator (regulation of crystallinity) under N₂ atmosphere (to prevent oxidation of dithiols) in *N,N*-diethylformamide (DEF)/H₂O mixture at 120 °C for 48 h gave isomorphic 2D MOFs, **M-dcbdt** (M = Ni, Co, or Fe), in yields of 48–73% (for synthetic details, see ESI†). Single-crystal structures of these three **M-dcbdt** were successfully obtained by single-crystal X-ray diffraction (SCXRD), and they crystallize in orthorhombic lattice with the space group of *Pbcn* (No. 60).¹¹ The 2D network is composed of two types of metal node, metal-bis(dithiolene) ([MS₄]) and metal-centred octahedra ([M(COO)₄(H₂O)₂]) (Fig. 1c). Considering [MS₄] units, two benzenedithiolate planes form dihedral angles of 4.43–7.07° in the order of **Ni-dcbdt** < **Co-dcbdt** < **Fe-dcbdt**, in line with the trend of their M–S bond

^a School of Chemical Engineering and Light Industry, Guangdong University of Technology, Guangzhou 510006, P. R. China. E-mail: junhe@gdut.edu.cn

^b Guangdong Provincial Laboratory of Chemistry and Fine Chemical Engineering Jieyang Center, Jieyang 515200, China. E-mail: laihonchung@gdut.edu.cn

† Electronic supplementary information (ESI) available: Preparation details of **M-dcbdt** and metallolinkers, procedures for photocatalysis, and spectroscopic data, additional plots/figures. See DOI: <https://doi.org/10.1039/d4cc02282c>

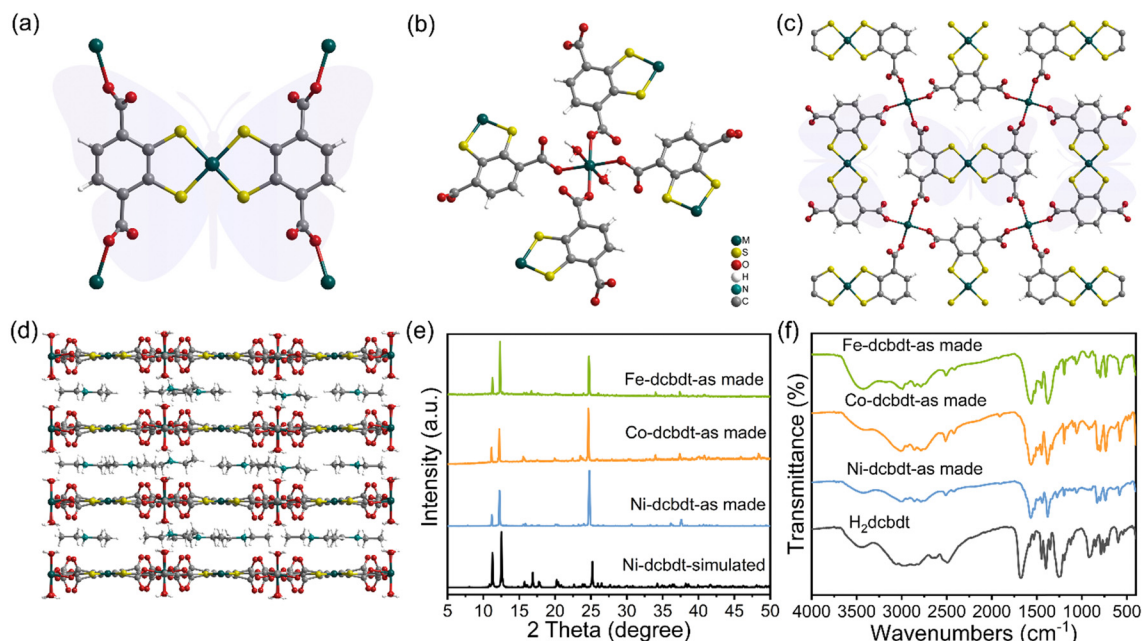


Fig. 1 Single-crystal structure of **M-dcbdt**: coordination environments of (a) $[MS_4]$ node and (b) $[M(COO)_4(H_2O)_2]$ node; (c) 2D network viewed along the c axis; (d) stacking of 2D **M-dcbdt** and $Et_2NH_2^+$ layers. (e) PXRD patterns of as-made **M-dcbdt** and single crystal of **Ni-dcbdt**. (f) FT-IR spectra of **M-dcbdt** and H_2dcbdt .

distances ($Ni-S$: 2.149–2.155 Å < $Co-S$: 2.163–2.170 Å < $Fe-S$: 2.197–2.202 Å). Plausibly weaker chelation of dithiolate to the metal centre allows a higher degree of fluxional behaviour of benzenedithiolate moieties. The $[MS_4]$ units order perpendicularly in alternate manner, with all $-COO^-$ apexes twisted (dihedral angles between two opposite $-COO^-$ found to be 54.43–58.47°), forming butterfly-shaped connectors for coordinating another type of metal centre in monodentate fashion to give octahedral nodes bearing four equatorial $-COO^-$ and two axial aqua ligands (Fig. 1a). In other words, butterfly-shaped $[MS_4]$ linkers connect to the $([M(COO)_4(H_2O)_2])$ node to form a 4,4- c net (Fig. 1b). Noteworthy, diethylammonium ($Et_2NH_2^+$) ions, probably originating from the decomposition of DEF, are trapped in the interlayer cavity for charge balance, signifying the anionic nature of the main framework. All **M-dcbdt** complexes possess identical asymmetric units of $[M_2(dcbdt)_2(H_2O)_2(Et_2NH_2)_3]$, and two metal centres are needed to neutralize a total of five negative charges, suggesting the coexistence of M^{II} and M^{III} species.

It is worth noting that butterfly-shaped $[MS_4]$ metallolinkers could be prepared by same reaction conditions with a shorter duration (24 h); the Ni-analogue has been resolved crystallographically.¹¹ Again, $Et_2NH_2^+$ ions were found in molecular crystals, highlighting the anionic nature of the $[MS_4]$ linkers. Interestingly, compared with those of **M-dcbdt**, the $[NiS_4]$ molecule possesses larger dihedral angles between two opposite $-COO^-$ terminals (68.98°) and between benzenedithiolate planes (11.94°) (Fig. S1, ESI†). The lack of octahedral $([M(COO)_4(H_2O)_2])$ nodes to fix benzenedithiolate portions possibly accounts for divergent dihedral angles. Importantly, the butterfly-shaped $[MS_4]$ metallolinkers could assemble **M-dcbdt** through reaction with respective metal salts in DEF/ H_2O mixture at 120 °C for 48 h, highlighting the intermediacy of the $[MS_4]$ metallolinkers.

The powder X-ray diffraction (PXRD) patterns of **M-dcbdt** match well with PXRD patterns simulated from single-crystal data, confirming the phase purity of as-made samples (Fig. 1e). The retained PXRD patterns of **M-dcbdt** in different solvents (organic and aqueous solutions) and thermogravimetric analysis (TGA) revealed the satisfactory chemical and thermal stability of **M-dcbdt** (Fig. S3 and S4, ESI†), which are conducive to the investigation of their photocatalytic properties. As shown in Fourier transform infrared (FT-IR) spectra, a great drop in stretching signal at around 2500 cm^{-1} from H_2dcbdt to **M-dcbdt** comes from the consumption of S–H bond for the formation of metal-bis(dithiolene) (Fig. 1f). As shown in scanning electron microscope (SEM) images and energy dispersive X-ray spectroscopy (EDS), all MOFs are in block or pillar morphology, with even distribution of S and metal over the framework (Fig. S5–S7, ESI†). When it comes to $[MS_4]$ moieties, electrical conductivity always captures one's attention. **M-dcbdt** exhibited fair electrical conductivity of 10^{-8} – 10^{-6} S cm^{-1} , plausibly stemming from interrupted e^- transport by octahedral metal nodes.

To probe the chemical environment of the metal centres and sulphur in **M-dcbdt**, high-resolution X-ray photoelectron spectroscopy (XPS) was employed. Fine spectra of S in **M-dcbdt** also gave three sets of signals. Peaks in the range of 162–162.24 and 163.17–163.42 eV correspond to $2p_{3/2}$ and $2p_{1/2}$ of $M-S^-$, respectively, which are similar to the $M-S^-$ of metal-dithiolene moieties probed in the UiO-66 framework;¹² noteworthy, signals of oxidized S were probed in **Fe-dcbdt** and **Co-dcbdt**, probably coming from the drawing of e^- density from thiolate to the metal centres, oxidation of S to $S=O$ or formation of $-S^\bullet$ arising from strong backdonation of e^- by $-S^-$ to M centres (Fig. 2a and b and Fig. S8–S10, ESI†). Importantly, all **M-dcbdt** showed M $2p_{3/2}$ and $2p_{1/2}$ signals of divalent and

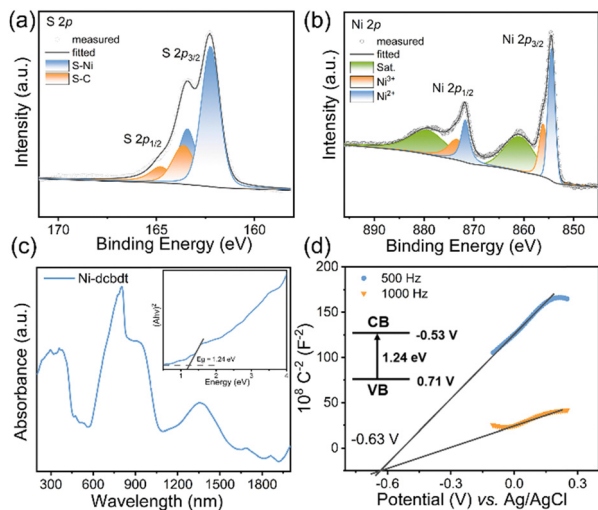


Fig. 2 XPS analysis: (a) S 2p and (b) Ni 2p of **Ni-dcbdt**. (c) Absorption profile and (d) M–S plot of **Ni-dcbdt**.

trivalent states (Ni^{II} : 854.45 and 871.65 eV; Ni^{III} : 856.21 and 873.6 eV; Co^{II} : 780.18 and 795.98 eV; Co^{III} : 782.19 and 798.57 eV; Fe^{II} : 708.82 and 722 eV; and Fe^{III} : 710.38 and 723.56 eV), signifying the mixed valency (*i.e.*, M^{2+} and M^{3+}) of metal centres.

Light absorption capacity and band structure are key parameters for evaluating the suitability of a photocatalyst towards a specific type of photocatalysis. Notably, UV-visible diffuse reflectance spectroscopy (UV-vis DRS) revealed that all **M-dcbdt** exhibit strong absorption covering the whole UV-vis region, along with moderate absorption reaching the near-IR spectral region (Fig. 2c and Fig. S11, ESI[†]). By Kubelka–Munk (K–M) conversion, the band gaps of **Ni-dcbdt**, **Co-dcbdt** and **Fe-dcbdt** were estimated to be 1.24, 1.5 and 1.54 eV, respectively (Fig. 2c and Fig. S12, ESI[†]). Mott–Schottky (M–S) measurements gave **M-dcbdt** curves of positive slope, revealing the n-type semiconducting nature of **M-dcbdt**. The flat band potentials of **Ni-dcbdt**, **Co-dcbdt** and **Fe-dcbdt** were found to be -0.63 , -1.27 and -0.27 V vs. Ag/AgCl, respectively (Fig. 2d and Fig. S13, ESI[†]). Since the conduction band (CB) edge is more negative than the measured flat band potential in n-type semiconductors,¹³ the CB edges of **Ni-dcbdt**, **Co-dcbdt** and **Fe-dcbdt** were estimated to be -0.53 , -1.17 and -0.17 V vs. normal hydrogen electrode (NHE) at pH = 7, respectively (Fig. 2d and Fig. S13, ESI[†]). As a result, the valence band (VB) edges of **Ni-dcbdt**, **Co-dcbdt** and **Fe-dcbdt** were calculated to be 0.71, 0.33 and 1.37 V vs. NHE at pH = 7, respectively (Fig. 2d and Fig. S13, ESI[†]). Higher-lying CB edges of **Ni-dcbdt** and **Co-dcbdt** than $\text{E}(\text{H}^+/\text{H}_2)$ (-0.41 V vs. NHE at pH = 7) signify their potential in photocatalytic HER.

Considering the solvent stability, broad absorption range as well as appropriate band structures, **M-dcbdt** were evaluated for photocatalytic HER performance under visible-light irradiation ($\lambda_{\text{ex}} \geq 420$ nm, illumination intensity = 405 mW cm^{-2} , reactor area = 7.06 cm^2) in *N,N*-dimethylformamide (DMF)/ H_2O (5 mL, 1:1, v/v), using $[\text{Ru}(\text{bpy})_3]\text{Cl}_2$ as a photosensitizer and *N,N*-dimethylaniline as a scavenger. Given that all **M-dcbdt** possess CB edges lower-lying than the lowest unoccupied molecular

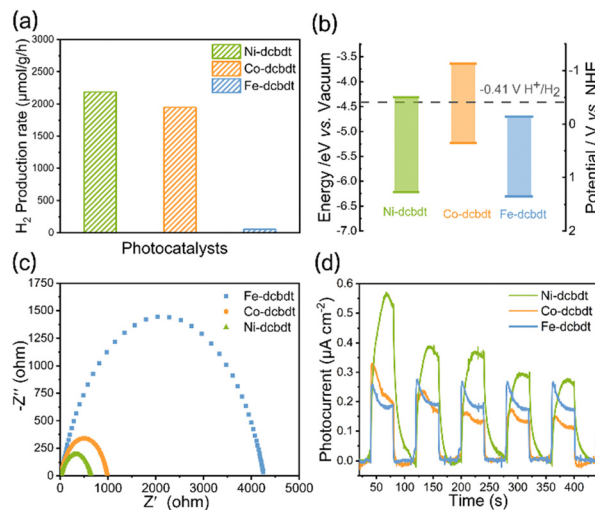


Fig. 3 (a) Rate of photocatalytic H_2 evolution of **M-dcbdt**. (b) Band structures of **M-dcbdt**. (c) Nyquist plots of EIS and (d) photocurrent responses of **M-dcbdt**.

orbital (LUMO) of $[\text{Ru}(\text{bpy})_3]^{2+}$, photogenerated e^- manage to migrate from photoexcited $[\text{Ru}(\text{bpy})_3]^{2+}$ to the CB edges of **M-dcbdt** for the HER. Among all **M-dcbdt** studied in this work, **Ni-dcbdt** gave the highest HER rate of $2189 \mu\text{mol g}^{-1} \text{h}^{-1}$, better than those of **Co-dcbdt** ($1948 \mu\text{mol g}^{-1} \text{h}^{-1}$) and **Fe-dcbdt** ($54.3 \mu\text{mol g}^{-1} \text{h}^{-1}$) (Fig. 3a). The closest-lying CB edge of **Ni-dcbdt** (-0.53 V vs. NHE, pH = 7) to $\text{E}(\text{H}^+/\text{H}_2)$ (-0.41 V vs. NHE, pH = 7) probably accounts for its best HER rate. On the contrary, the far higher-lying CB edge of **Co-dcbdt** (-1.17 V vs. NHE, pH = 7) still retains weaker HER performance, but the far lower-lying CB edge of **Fe-dcbdt** leads to energetically inadequate photogenerated e^- for the HER and hence shows negligible HER performance. Notably, **M-dcbdt** did not show HER performance without $[\text{Ru}(\text{bpy})_3]\text{Cl}_2$, attributed to the lack of inherent photosensitizing capacity of **M-dcbdt**.

To further rationalize the photocatalytic process of **M-dcbdt**, electrochemical impedance spectroscopy (EIS) and transient photocurrent response were employed to study **M-dcbdt**. EIS plots show signal radii in the ascending order of **Ni-dcbdt** < **Co-dcbdt** < **Fe-dcbdt** (Fig. 3b), indicative of increasing charge transfer resistance (*i.e.*, decreasing charge transfer rates). Conversely, transient photocurrent response follows the order of **Ni-dcbdt** > **Co-dcbdt** > **Fe-dcbdt** (Fig. 3c), indicating the order of charge separation efficiency. These results are in line with the HER rate (**Ni-dcbdt** > **Co-dcbdt** > **Fe-dcbdt**) and collectively support the best HER performance by **Ni-dcbdt**.

Photoirradiation of $[\text{Ru}(\text{bpy})_3]\text{Cl}_2$ produces the photoexcited state $[\text{Ru}(\text{bpy})_3]^{2+*}$, which can be quenched either through reductive mechanism (reduced by e^- donor) or oxidative mechanism (oxidised by e^- acceptor). As shown in Fig. S14 (ESI[†]), the photoluminescence of $[\text{Ru}(\text{bpy})_3]^{2+}$ was quenched quantitatively by **Ni-dcbdt**, suggesting **Ni-dcbdt** as an oxidative quencher for $[\text{Ru}(\text{bpy})_3]^{2+*}$. Specifically, upon photoexcitation, $[\text{Ru}^{\text{II}}(\text{bpy})_3]^{2+}$ transforms to $[\text{Ru}^{\text{III}}(\text{bpy})_2(\text{bpy}^{\bullet-})]^{2+*}$, which has a LUMO (-1.26 V vs. NHE, pH = 7) higher-lying than the CB edge of **Ni-dcbdt** (-0.53 V vs.

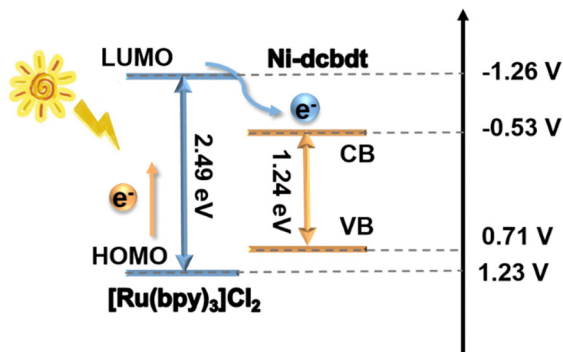


Fig. 4 Scheme showing the photoexcitation of $[\text{Ru}(\text{bpy})_3]^{2+}$ and e^- migration from the LUMO of $[\text{Ru}(\text{bpy})_3]^{2+}$ to the CB of **Ni-dcbdt**.

NHE, pH = 7) (Fig. 4). Migration of photogenerated e^- from $[\text{Ru}^{\text{III}}(\text{bpy})_2(\text{bpy}^{\bullet-})]^{2+*}$ to the CB edge of **Ni-dcbdt** produces $[\text{Ru}^{\text{III}}(\text{bpy})_3]^{3+}$ and **Ni-dcbdt** $^{\bullet-}$, responsible for the oxidation of scavengers and reduction of H^+ to H_2 , respectively. The photocatalytic HER mechanism for **Co-dcbdt** with $[\text{Ru}(\text{bpy})_3]^{2+}$ as a photosensitizer is the same, only with **Co-dcbdt** bearing a higher-lying CB edge.

In short, our work demonstrated dithiol-dicarboxylic acid (**H₂dcbdt**) as a simple building block to assemble a 2D MOF (**M-dcbdt**; M = Ni, Co or Fe) comprising unprecedented butterfly-shaped tetratopic metal-bis(dithiolene) $[\text{MS}_4]$ linkers in one-pot manner. With satisfactory solvent stability, broad absorption range and reductive $[\text{MS}_4]$ sites, **M-dcbdt** demonstrated catalytic activity in visible-light-driven HER, with **Ni-dcbdt** exhibiting the highest HER rate of $2189 \mu\text{mol g}^{-1} \text{h}^{-1}$. This work offers an easy access towards metal-bis(dithiolene)-based networks and opens an opportunity for more in-depth study of MOFs bearing functional metal-bis(dithiolene) units.

This work was supported by the National Natural Science Foundation of China (22371054 and 22301045), Foundation of Basic and Applied Basic Research of Guangdong Province (2020B1515120024 and 2024A1515012801), and Science and Technology Planning Project of Guangdong Province (2021A0505030066 and 2023A0505050164). We also thank the Instrumental Analysis Centre of Guangdong University of Technology for single-crystal data, SEM images collection, XPS and photoluminescence measurement.

Data availability

The data supporting this article have been included as part of the ESI.† Crystallographic data for **M-dcbdt** and $[\text{NiS}_4]$ molecule have been published in CSD communication and can be obtained from: **Ni-dcbdt** (DOI: <https://doi.org/10.5517/ccdc.csd.cc2jy7zq>); **Co-dcbdt** (DOI: <https://doi.org/10.5517/ccdc.csd.cc2jy7yp>); **Fe-dcbdt** (DOI: <https://doi.org/10.5517/ccdc.csd.cc2jy7xn>); and $[\text{NiS}_4]$ molecule (DOI: <https://doi.org/10.5517/ccdc.csd.cc2jy9qj>).

Conflicts of interest

There are no conflicts to declare.

Notes and references

- R. Eisenberg and H. B. Gray, *Inorg. Chem.*, 2011, **50**, 9741–9751.
- J. Xie, S. Ewing, J.-N. Boyn, A. S. Filatov, B. Cheng, T. Ma, G. L. Grocke, N. Zhao, R. Itani, X. Sun, H. Cho, Z. Chen, K. W. Chapman, S. N. Patel, D. V. Talapin, J. Park, D. A. Mazziotti and J. S. Anderson, *Nature*, 2022, **611**, 479–484.
- (a) A. J. Clough, J. W. Yoo, M. H. Mecklenburg and S. C. Marinescu, *J. Am. Chem. Soc.*, 2015, **137**, 118–121; (b) C. A. Downes and S. C. Marinescu, *J. Am. Chem. Soc.*, 2015, **137**, 13740–13743; (c) J. Du, B. Cheng, H. Yuan, Y. Tao, Y. Chen, M. Ming, Z. Han and R. Eisenberg, *Angew. Chem., Int. Ed.*, 2023, **62**, e202211804.
- (a) H. Schindelin, C. Kisker, J. Hilton, K. V. Rajagopalan and D. C. Rees, *Science*, 1996, **272**, 1615–1621; (b) G. Schwarz, R. R. Mendel and M. W. Ribbe, *Nature*, 2009, **460**, 839–847.
- D. J. Cole-Hamilton, *Science*, 2003, **299**, 1702–1706.
- (a) T. Kambe, R. Sakamoto, K. Hoshiko, K. Takada, M. Miyachi, J.-H. Ryu, S. Sasaki, J. Kim, K. Nakazato, M. Takata and H. Nishihara, *J. Am. Chem. Soc.*, 2013, **135**, 2462–2465; (b) T. Kambe, R. Sakamoto, T. Kusamoto, T. Pal, N. Fukui, K. Hoshiko, T. Shimojima, Z. Wang, T. Hirahara, K. Ishizaka, S. Hasegawa, F. Liu and H. Nishihara, *J. Am. Chem. Soc.*, 2014, **136**, 14357–14360; (c) X. Huang, P. Sheng, Z. Tu, F. Zhang, J. Wang, H. Geng, Y. Zou, C.-A. Di, Y. Yi, Y. Sun, W. Xu and D. Zhu, *Nat. Commun.*, 2015, **6**, 7408; (d) A. J. Clough, J. M. Skelton, C. A. Downes, A. A. de la Rosa, J. W. Yoo, A. Walsh, B. C. Melot and S. C. Marinescu, *J. Am. Chem. Soc.*, 2017, **139**, 10863–10867; (e) J. Huang, Y. He, M.-S. Yao, J. He, G. Xu, M. Zeller and Z. Xu, *J. Mater. Chem. A*, 2017, **5**, 16139–16143; (f) L. S. Xie, G. Skorupskii and M. Dinca, *Chem. Rev.*, 2020, **120**, 8536–8580; (g) M. Wang, R. Dong and X. Feng, *Chem. Soc. Rev.*, 2021, **50**, 2764–2793; (h) X. Huang, S. Fu, C. Lin, Y. Lu, M. Wang, P. Zhang, C. Huang, Z. Li, Z. Liao, Y. Zou, J. Li, S. Zhou, M. Helm, P. S. Petkov, T. Heine, M. Bonn, H. I. Wang, X. Feng and R. Dong, *J. Am. Chem. Soc.*, 2023, **145**, 2430–2438; (i) J. Hu, J.-Z. Xiao, W.-M. Liao, S. Liu, J. Li, Y. He, L. Yu, Q. Li, G. Xu and J. He, *J. Mater. Chem. A*, 2023, **11**, 11463–11470; (j) J. Liu, G. Xing and L. Chen, *Acc. Chem. Res.*, 2024, **57**, 1032–1045; (k) S.-W. Ke, J. Xin, L. Tang, L. Gao, G. Cai, M. Ding, S. Yuan, J. Sun and J.-L. Zuo, *ACS Mater. Lett.*, 2024, **6**, 921–927.
- (a) Y. Zhou, Q. Hu, F. Yu, G.-Y. Ran, H.-Y. Wang, N. D. Shepherd, D. M. D'Alessandro, M. Kurmoo and J.-L. Zuo, *J. Am. Chem. Soc.*, 2020, **142**, 20313–20317; (b) X.-C. Zhou, C. Liu, J. Su, Y.-F. Liu, Z. Mu, Y. Sun, Z.-M. Yang, S. Yuan, M. Ding and J.-L. Zuo, *Angew. Chem., Int. Ed.*, 2023, **62**, e202211850.
- Y. Zhou, S. Liu, Y. Gu, G.-H. Wen, J. Ma, J.-L. Zuo and M. Ding, *J. Am. Chem. Soc.*, 2023, **145**, 6247–6256.
- (a) S.-W. Ke, Y. Wang, J. Su, K. Liao, S. Lv, X. Song, T. Ma, S. Yuan, Z. Jin and J.-L. Zuo, *J. Am. Chem. Soc.*, 2022, **144**, 8267–8277; (b) S.-W. Ke, W. Li, Y. Gu, J. Su, Y. Liu, S. Yuan, J.-L. Zuo, J. Ma and P. He, *Sci. Adv.*, 2023, **9**, eadf2398; (c) Y. Wang, S.-W. Ke, G. Qiao, J. Liang, X. Zhou, X. Song, Z. Tie, S. Yuan, J.-L. Zuo and Z. Jin, *Adv. Energy Mater.*, 2024, **14**, 2303051; (d) S. Lv, X. Ma, S. Ke, Y. Wang, T. Ma, S. Yuan, Z. Jin and J.-L. Zuo, *J. Am. Chem. Soc.*, 2024, **146**, 9385–9394.
- (a) Q. Gu, Z.-H. Zhao, B. Chan, T. Yan, J.-L. Zuo, D. M. D'Alessandro and C.-H. Li, *ACS Mater. Lett.*, 2023, **5**, 603–607; (b) T.-R. Ma, F. Ge, S.-W. Ke, S. Lv, Z.-M. Yang, X.-C. Zhou, C. Liu, X.-J. Wu, S. Yuan and J.-L. Zuo, *Small*, 2024, **20**, 2308013.
- Single crystal data were documented in CSD Communication as Experimental Crystal Structure Determination: **Ni-dcbdt** (DOI: 10.5517/ccdc.csd.cc2jy7zq); **Co-dcbdt** (DOI: 10.5517/ccdc.csd.cc2jy7yp); **Fe-dcbdt** (DOI: 10.5517/ccdc.csd.cc2jy7xn); $[\text{NiS}_4]$ molecule (DOI: 10.5517/ccdc.csd.cc2jy9qj).
- H. Zhong, S. Chen, Z. Jiang, J. Hu, J. Dong, L.-H. Chung, Q.-C. Lin, W. Ou, L. Yu and J. He, *Small*, 2023, **19**, 2207266.
- G.-Q. Lai, Z. Jiang, H. Zhong, L.-H. Chung, N. Li and J. He, *Chin. J. Struct. Chem.*, 2023, **42**, 100090.